

Manufacturing Letters

Manufacturing Letters 33 (2022) 133-142



50th SME North American Manufacturing Research Conference (NAMRC 50, 2022)

Hybrid manufacturing of Invar mold for carbon fiber layup using structured light scanning

Aaron Cornelius^a, Leah Jacobs^a, Matthew Lamsey^a, Logan McNeil^a, William Hamel^a, and Tony Schmitz^{a,b,*}

^aUniversity of Tennessee, Mechanical, Aerospace, and Biomedical Engineering Department, Knoxville, TN, USA
^bOak Ridge National Laboratory, Manufacturing Science Division, Oak Ridge, TN, USA

Abstract

This paper describes coordinate system definition and transfer for five-axis machining of additively-manufactured preforms. In this method, a set of fiducials are attached to the temporarily attached to the part, and their location relative to the preform geometry is calibrated using a structured light scanner. Those fiducials can then be measured in the machine tool to determine the location and orientation of the part. The method is demonstrated by finish-machining a carbon fiber layup mold from an additively manufactured Invar preform. In addition to showing the coordinate transfer methods necessary to machine the part, several key challenges with machining additively-manufactured preforms are discussed and potential solutions are proposed. Unfortunately, the final part was ultimately unusable due to porosity inside the part left from the additive process. Future work will remanufacture this part while taking steps to avoid porosity and other challenges encountered.

© 2022 Society of Manufacturing Engineers (SME). Published by Elsevier Ltd. All rights reserved. This is an open access article under the CC BY-NC-ND license (http://creativecommons.org/licenses/by-nc-nd/4.0/) Peer-review under responsibility of the Scientific Committee of the NAMRI/SME. *Keywords:* Additive manufacturing; Milling; Structured light scanning; Metrology; Fiducials

1. Introduction

Hybrid manufacturing, combining additive material deposition and subtractive finish machining, is an increasingly common process for producing complex parts. However, one persistent problem is coordinate system transfer, i.e., identifying where the part should be located on the machining center to produce the desired geometry from the additive preform, the relative orientation and position between the additive preform and desired geometry required to produce a usable final part, and the associated toolpaths. This problem is particularly difficult for five-axis machining because both the orientation and translation of the part must be identified.

Traditional methods for coordinate system transfer rely on locating a small number of points on the part using a touch probe. However, this process is difficult for hybrid manufacturing because: 1) hybrid parts tend to be geometrically complex and lack simple prismatic reference features that can be used to locate the part and establish datums; and 2) additive processes can exhibit significant deviations between the desired and the as-printed geometry. Some methods work around this by probing a large number of points on the part and creating a best-fit alignment, but this method is time-consuming, requires having an accurate model of the preform geometry, and can still only incorporate a limited amount of the part surface (e.g., [1]). Other authors have proposed fiducial-based methods which mount a set of easily-measured features to a part and calibrate their position relative to the part geometry using a CMM. These fiducials can then be measured on the machine to determine the location of the part. While this minimizes probing time on-themachine, this method is still time-consuming and difficult to apply to large freeform parts.

^{*} Corresponding author at: University of Tennessee, Mechanical, Aerospace, and Biomedical Engineering Department, Knoxville, TN, USA. E-mail address: tony.schmitz@utk.edu (T. Schmitz).

Previous work has demonstrated that structured light scanning can replace the CMM for calibrating the part-mounted fiducial positions [2]. Compared with traditional fiducial methods, this has several advantages. First, it can incorporate the entire geometry of the preform to determine the optimal alignment, not just a small subset of points. Second, the scanning yields a model of the full preform geometry which can be used to optimize toolpaths and reduce cycle time. Third, scanning does not require CMM programming and can quickly capture large or awkwardly shaped parts.

To date, this fiducial/scanning method has been applied to 3d milling of simple geometries. This paper examines how the method can be extended to full 5-axis machining of complex real-world parts, using a carbon fiber layup mold (shown in Figure 1) as a case study to showcase the benefits and limitations of the proposed method. The preform for this mold was produced by Lincoln Electric using wire are additive manufacturing. A previous attempt to machine this part by a separate group failed and scrapped the part because they couldn't accurately find the required position and orientation of the part in the machine (see [3] for details on the design, printing, and first machining attempt for this part). Applying the fiducial/scanning method overcomes this challenge and allowed for successful machining.

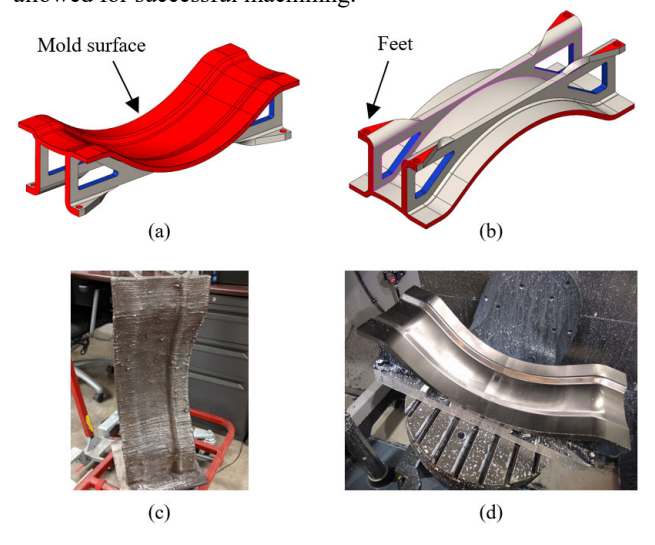


Figure 1. (a, b) Nominal CAD model for the mold. Gray areas were left asprinted. Red areas required finish machining. Blue areas were waterjet cut after machining. (c) Printed preform before removal from the build plate. (d) Fully machined mold. The overall part dimensions were 660 mm by 250 mm by 170 mm.

Unfortunately, the final machined part was unusable due to porosity in the part which left voids on the mold surface. Work is ongoing for a second iteration to correct this issue. As a result, this paper serves as an initial case-study of the ways that the fiducial/scanning method can facilitate finish machining of additively-manufactured preforms, and several important conclusions are drawn to help further improve the machining process for the next iteration of this project.

The remainder of the paper is organized as follows. Section 2 reviews the current literature for finish-machining of additively-manufactured preforms, structured light scanning, and fiducial-based methods for coordinate system transfer. Sections 3-5 step through the process of scanning the preform,

attaching fiducials and measuring their position relative to preform, and completing the coordinate system transfer. Section 6 analyzes the accuracy of the final machined part and discusses the causes for various deviations from the desired geometry. Section 7 discusses the results and makes suggestions for future work.

2. Prior research

2.1. Hybrid manufacturing

Generally, hybrid manufacturing is defined as a combination of manufacturing processes to produces parts in a more optimal fashion. A key area of study is the combination of additive and subtractive manufacturing (machining). Recent review papers describe the current state-of-the-art for hybrid manufacturing [4-5].

Prior efforts have studied methods for finish machining printed parts. Stavropoulos et al. investigated the machinability of directed energy deposition preforms, analyzing tool wear and surface quality [6]. Chen et al. studied how parametric features of the part model could be used to automatically plan machining toolpaths for four axis finish machining [7]. Liou et al. described a case of powder-based laser metal deposition + CNC milling in a single machine [8]. They defined an automated process planning sequence composed of determining the base face (which functioned as the machining fixture), extracting the part skeleton, decomposing a part into subparts, determining build sequence and direction for subparts, checking the feasibility of the build sequence and direction for the machining process, and optimization of the deposition and machining steps. Yamazaki described the combination of laser metal deposition, turning, and milling capabilities in a single, commercial machine [9]. Advantages were increased functionality and flexibility for small lot production runs. Disadvantages include heat transfer into the machine structure from the laser deposition, which can limit accuracy, and the combination of powder (for deposition) and coolant (for machining) in the same work volume. Song et al. explored early process development of WAAM + CNC milling in a single machine [10]. They described a retrofit of gas metal arc welding (GMAW) on a three-axis milling machine to enable both high rate deposition and material removal to obtain the required surface finish. The setup included a heated build plate to reduce residual stress during deposition. Cornelius et al. first described the framework for the temporary fiducial and structured light scanning approach for three-axis machining implemented here for five-axis machining [2].

2.2. Structured light scanning

Structured light scanning is a well-established method for generating three-dimensional part models. A selected pattern of light is projected onto the part. The pattern is distorted by the geometry of the part and the resulting images are captured by (typically) two cameras from different angles. If the relative spatial position of the cameras is known, then the images can be analyzed to reconstruct the geometry. If a part is too large to

be captured in a single scan, multiple overlapping scans can be combined to generate a model of the entire part.

The accuracy of this method has been analyzed by several authors. Eiríksson *et al.* studied how calibration methods affect the accuracy of scanners [11]. Gebler *et al.* compared the performance of structured light scanning to photogrammetry by measuring artifacts and comparing the scans to the known artifact geometry [12]. Gandhali *et al.* demonstrated that kinematic couplings can be used to analyze the accuracy of a structured light scanner by moving an artifact in a repeatable way [13]. Cornelius *et al.* analyzed the repeatability of the scanned fiducial coordinate system based on repeated scans [2].

2.3. Fiducials for coordinate system transfer

Fiducial markers have been widely used for part and coordinate identification in a large variety of applications, such as medical components and printed circuit board design [14, 15]. Several studies have used fiducial systems to locate parts and calibrate machine tools. Smith et al. demonstrated the fiducial calibration system, where that the position of fiducials on a part are calibrated using a coordinate measurement machine (CMM). Those calibrated positions are measured on the machine tool and used to adjust machining toolpaths to compensate for part position and orientation, thermal expansion, and simple machine geometric errors [16]. This approach was developed for large monolithic workpieces such as aerospace structures. A similar concept was reported by Wang et al. for manufacturing precision freeform optics [17]. Liu et al. extended on these methods to enable local corrections in different areas of the part, compensating for local deformations in the workpiece [18].

Other authors have applied fiducials specifically to machining additively manufactured preforms. Srinivasan *et al.* performed an initial study for locating additively manufactured preforms on a four-axis machine tool by scanning them inside of a machining center with a laser scanner [19]. By placing fiducials inside of the machine that were captured in the same scan as the part, they were able to identify the rough position and orientation of a rectangular block inside of the machine.

Cornelius *et al.* demonstrated that part-mounted fiducials and structured light scanning can be used to machine parts [2]. The scan was used to determine the optimal position and orientation of the CAD and preform geometry while considering geometric constraints imposed by the machine tool. A coordinate system was established based on the fiducials and used to program the part. The coordinate system was reconstructed inside of a three-axis CNC machining center by probing the fiducials and that coordinate system was used to machine the component. This paper extends these previous efforts by applying the fiducial concept to five-axis machining and demonstrating how it can provide improved part quality and reduced cycle time.



Figure 2. Initial preform scan after removal from the WAAM build plate.

3. Scanning and alignment

The first step in machining was to create a scan of the initial preform after it was removed from the WAAM build plate. The part was scanned using a GOM ATOS Q structured light scanner. The initial scan is shown in Figure 2.

This scan was used to determine the optimal relative position and orientation between the CAD model and the preform (generally referred to as the alignment step). The alignment was set using GOM Inspect software to identify the local best fit with tolerances function; see Figure 3. This function performs a least-squares best fit alignment, but also allows the user to specify minimum or maximum distances between specific surfaces on the CAD and scanned models. In order to ensure that the mold surface would be fully contained within the preform, the tolerance was selected to require the scanned model to be outside of the nominal CAD at all locations. This ensured that the CAD is fully contained in the preform and that the nominal geometry can be produced by machining (or if that is not possible, maximizes the amount of the CAD that is fully contained).

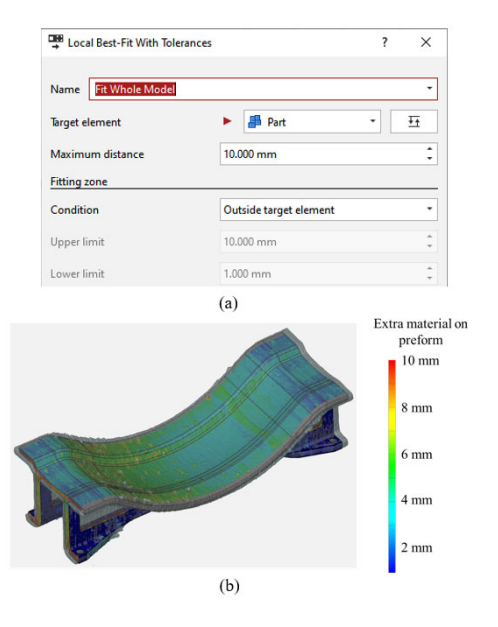


Figure 3. (a) GOM Inspect Local Best-Fit With Tolerances function for aligning the CAD and scan. The software finds the position that minimizes root-mean-squared distance error while ensuring that the part is contained inside the preform. (b) Initial alignment of the CAD model and preform. The color bar shows the deviation between the two models: red indicates that there is 10 mm of extra material on the preform compared to the nominal design, while blue indicates that there is no extra material.

Some areas on the feet and legs were not contained in this alignment, but this was acceptable because the full mold surface was contained with a minimum of 2 mm of extra material and the feet and legs are support structures only for the mold. The aligned model was then exported as an STL file using the CAD coordinate system. However, this STL file could not be used as a stock model for CAM since it doesn't form a single watertight mesh. Figure 4 shows some floating polygons that would cause the stock calculations to fail. Additionally, the scan included far higher resolution than necessary, which would have resulted in high calculation time.

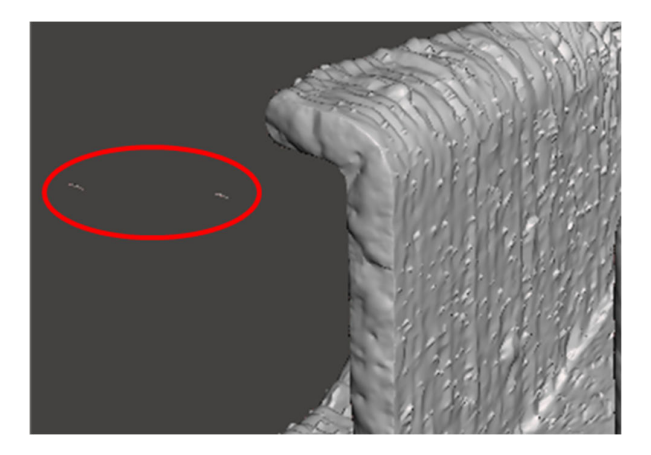


Figure 4. Initial scan exported as an STL. Note the floating geometry.

To obtain a watertight model, the STL was remeshed and down-sampled in Autodesk's Meshmixer software using the Make Solid tool with the highest solid accuracy and mesh density options. This closed all holes, removed floating geometry, and reduced the file size from 488 MB to 96 MB while still maintaining acceptable resolution. The settings and resulting mesh are shown in Figure 5Figure 5.

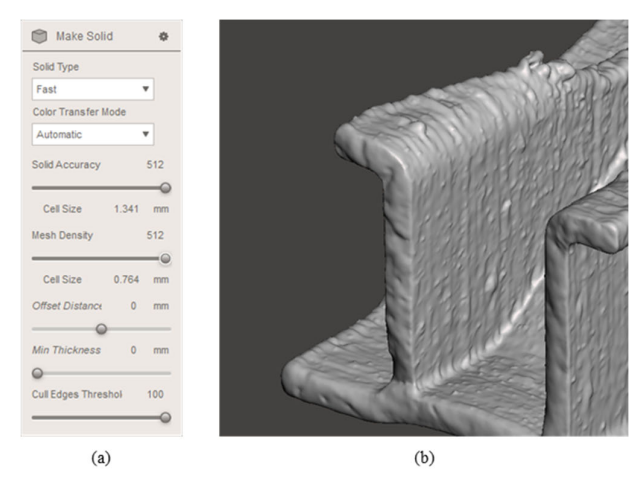


Figure 5: (a) Settings for Meshmixer's Make Solid tool. (b) Watertight STL after post-processing. A comparison to Figure 4 shows that the overall geometry is similar, but small features such as weld spatter have been smoothed by the decreased resolution.

The watertight STL and CAD model were then imported into the CAM software. Since the STL was exported using the CAD model coordinate system, the two were imported in the

desired positions relative to each other. The toolpaths were then planned using these models as shown in Figure 6. Roughing toolpaths were generated using the actual stock model to determine where material needed to be removed. Since toolpaths are only generated in the specific areas where material needs to be removed, cycle time can be reduced significantly over a more traditional approach which assumes a set amount of excess stock on the entire part surface.

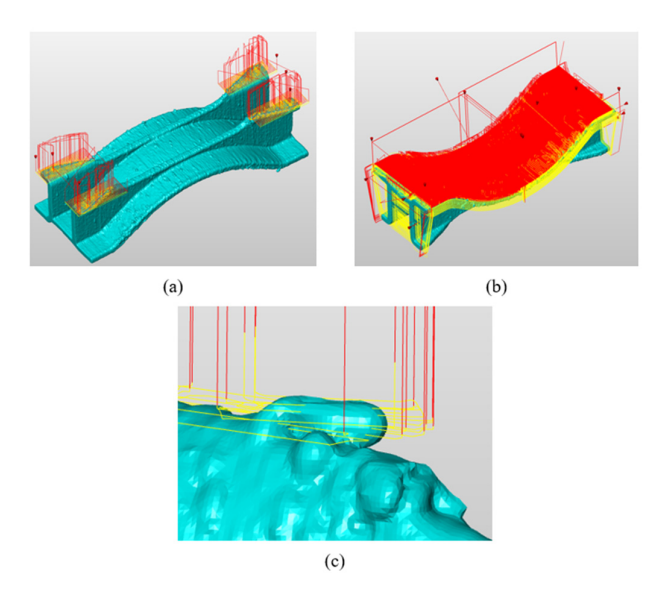


Figure 6. (a) Toolpaths for the first operation to machine the feet. (b)
Toolpaths for the second operation to machine the mold surface and edges.
(c) Closeup of roughing toolpaths. Additional cutting moves (yellow lines) are generated to remove the larger beads of extra material on the surface of the part.

4. Fiducial attachment and alignment

Next, fiducials were added to the part to transfer the coordinate system for the first machining operation (see Figure 7). These fiducials were 25.4 mm diameter satin-finished gage spheres (Bal-tec SAT-B100). These are commonly used for optical scanning calibration since the matte finish provides an effective scan surface. Three spheres were glued to the part with cyanoacrylate adhesive. Polymer printed tripods were used to increase the contact area between the spheres and the part. Once the spheres were attached, a small section of the part around the spheres was rescanned.

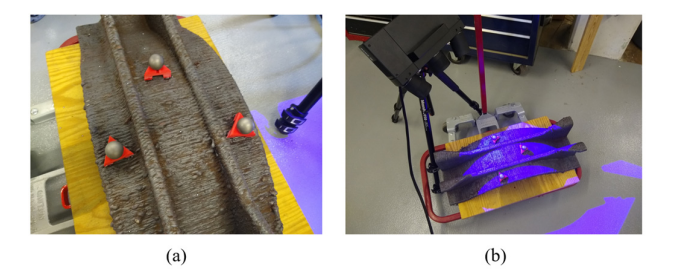


Figure 7. (a) Fiducial spheres mounted on part. (b) Scanning the area around the fiducial spheres.

The partial scan was then best fit to the original scan of the part, locating the three fiducial spheres relative to the original scan. Primitive elements were fit to these three spheres using a Gaussian least-squares method with a one standard deviation filter; see Figure 8.

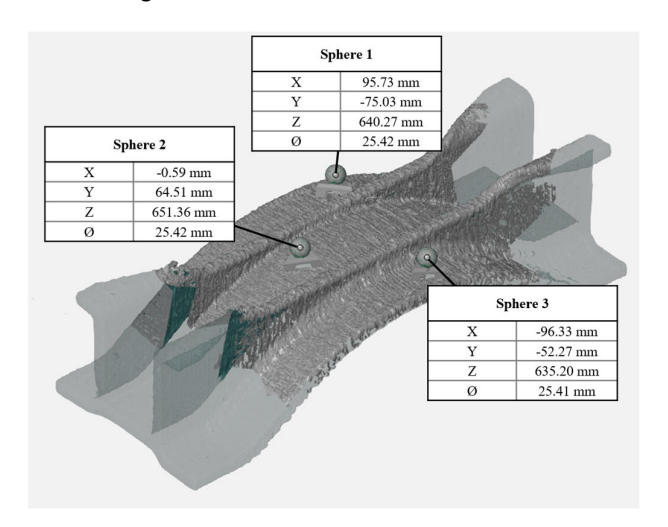


Figure 8. Partial scan with fiducials fit to the full initial scan. The initial scan is partly transparent. The measured locations and sizes of the three fiducial spheres are also shown. For reference, the nominal diameter (\varnothing) and tolerance for the spheres are 25.4 mm \pm 2.5 μ m.

The best fit centers of these geometric elements relative to the full scan were then transferred into CAM and used to define a fiducial coordinate system with orientation matrix $\boldsymbol{O}_{fiducial}$ and position vector $\boldsymbol{P}_{fiducial}$. The coordinate system is identified in Figure 9Figure 9. One point was arbitrarily selected as the origin, the second point defined the X axis, and the third point defined the XY plane.

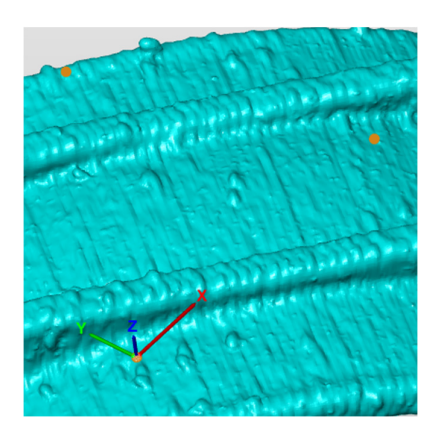


Figure 9. Fiducial coordinate system in CAM. Orange dots are the center points of the fiducial spheres used to define the coordinate system.

5. Locating the part and machining simulation

The part was clamped to the machine table and the three spheres were probed to find their center coordinates; see Table 1. These spheres define the fiducial coordinate system in machine coordinates $\mathbf{0}_{fid}^{mach}$, \mathbf{P}_{fid}^{mach} . Equations 1 through 5 show the mathematical derivation. The MATLAB code used to perform these transformations is provided in the appendix.

$$\boldsymbol{P}_{fid}^{mach} = \boldsymbol{P}_1 \tag{1}$$

$$X_{fid}^{mach} = \frac{P_2 - P_1}{\|P_2 - P_1\|} \tag{2}$$

$$Y_{fid}^{mach} = \frac{(\boldsymbol{P}_3 - \boldsymbol{P}_1) - \left((\boldsymbol{P}_3 - \boldsymbol{P}_1) \cdot \boldsymbol{X}_{fid}^{mach}\right) \cdot \boldsymbol{X}_{fid}^{mach}}{\left\|(\boldsymbol{P}_3 - \boldsymbol{P}_1) - \left((\boldsymbol{P}_3 - \boldsymbol{P}_1) \cdot \boldsymbol{X}_{fid}^{mach}\right) \cdot \boldsymbol{X}_{fid}^{mach}\right\|}$$
(3)

$$\mathbf{Z}_{fid}^{mach} = \mathbf{X}_{fid}^{mach} \times \mathbf{Y}_{fid}^{mach} \tag{4}$$

$$\mathbf{0}_{fid}^{mach} = \begin{bmatrix} \mathbf{X}_{fid}^{mach} & \mathbf{Y}_{fid}^{mach} & \mathbf{Z}_{fid}^{mach} \end{bmatrix}$$
 (5)

Table 1. Fiducial sphere center locations in machine coordinates

Sphere #	Vector	X (mm)	Y (mm)	Z (mm)
1	P_1	-401.589	-158.267	-339.596
2	P_2	-306.846	-298.259	-322.450
3	P_3	-209.784	-183.371	-343.326

The next step was to create the work coordinate system (WCS) to be shared between the machine and CAM software. The XYZ axes of this coordinate system were parallel to the machine tool axes and the origin was set at the center of sphere 1. On the machine controller side, this was completed by setting the WCS at the center of fiducial 1. The WCS was then reconstructed in CAM. The machine coordinate system was projected into the fiducial sphere coordinate system by inverting the fiducial coordinate frame. Since the orientation matrix is homogenous, this was done by transposing the matrix.

$$\boldsymbol{O}_{machine}^{fiducial} = \boldsymbol{O}_{fiducial}^{machine^{-1}} = \boldsymbol{O}_{fiducial}^{machine^{T}}$$
 (6)

The columns of this coordinate system defined the unit vectors along the X, Y, and Z axes of the machine frame within the fiducial coordinate system. The WCS was then reconstructed by creating points along those vectors and using them to define the WCS. The fiducial and machine coordinate systems are identified in Figure 10.

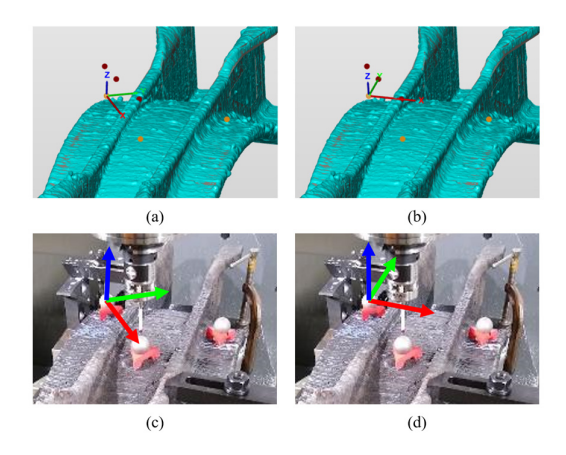


Figure 10. Comparison between the fiducial (a, c) and machining (b, d) coordinate systems in CAM (a, b) and on the machine (c, d). Orange dots in the CAM model are the positions of the fiducial sphere centers. Red dots in the CAM model are points on the machine X, Y, and Z axes.

The clamping position was set in CAM. This value is an offset between the WCS and the center of the machine tool table and is used by the CAM simulation to position the part inside of the simulated machine tool. Since the position of the center of the table on the machine relative to the machine's origin is known, it was straightforward to calculate and reconstruct in CAM. The clamping position is shown relative to the WCS in Figure 11.

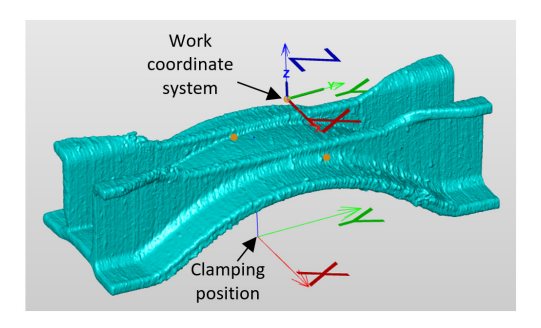


Figure 11. Clamping position in CAM, defined as an offset from the WCS to the center of the machine tool table

This single WCS was used for 3+2 axis machining using Dynamic Work Offsets (DWO). This is a function on Haas machine tools where the work offset is automatically translated and rotated in order to stay fixed relative to the part as the rotary axes move. The equivalent for simultaneous five-axis machining would be Tool Center Point Control (TCPC). Most five-axis machine controllers have similar functions. These functions are automatically activated in Hypermill's postprocessor and are thus transparent to the machine operator.

Next, the Hypermill CAM simulation was executed to validate the toolpaths. This checks for collisions and simulates material removal to make sure that the part will be machined correctly. Figure 12 displays a screenshot from the simulation. Note that the fixture wasn't modelled for this operation since there were no concerns about collision.



Figure 12: Simulation for feet machining

The simulation was critical for the first machining operation due to the large size of the part. If the part was set at certain angles the machine would not have sufficient travel to machine the required features. Simulating in CAM using the actual position allowed for the setup to be evaluated and the part adjusted until a good setup was identified. Once a good setup was found, the feet were machined.

The fiducials were then removed from the part and reattached on the mold surface side. The same process was used to set up and transfer the WCS, validate the machining process, and machine the part. There was only one notable change to the machining process. After roughing, voids from the printing process were identified on the part surface. Since voids are more common at the outer edges of the weld beads, it was decided to machine the mold surface 1 mm deeper than nominal on the CAD model to remove the surface layer. Figure 13 shows photographs from the machining sequence. The total machining time for both operations was 12.5 hours.

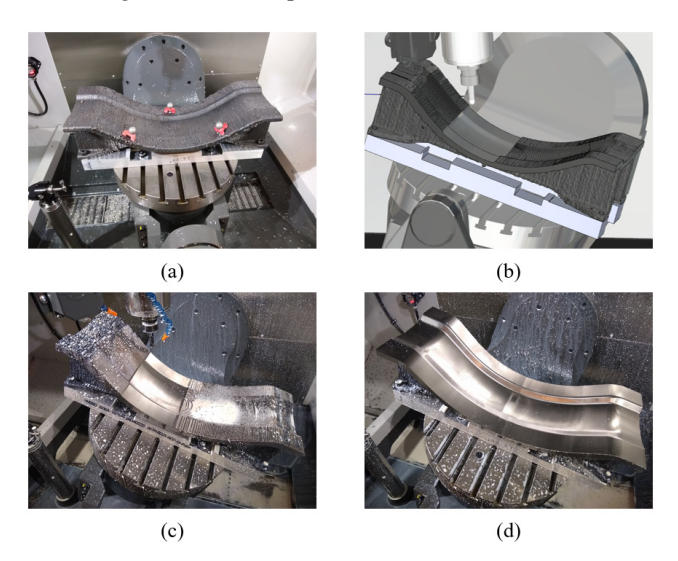
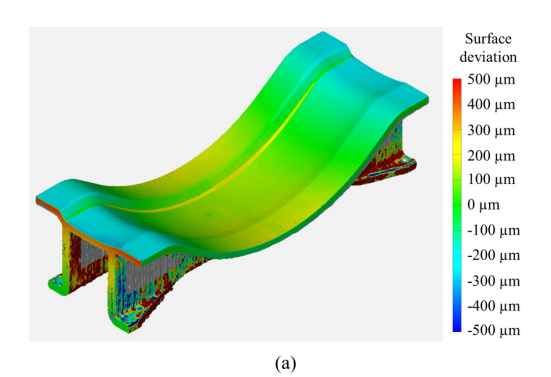


Figure 13. (a) Fiducials mounted on mold surface. (b) Simulation of finish machining. (c) Finish machining. (d) Fully machined part.

6. Dimensional analysis

After the part was fully machined, it was removed from the machine and scanned. An anti-glare spray (Krylon K01310) was applied to the machined surfaces to reduce specular reflection and improve scan results. The scan model was compared to both the nominal CAD model (Figure 14) and the predicted post-machining geometry from the CAM simulation (Figure 15). Note that this comparison was done before the leg cutouts were removed by waterjet.



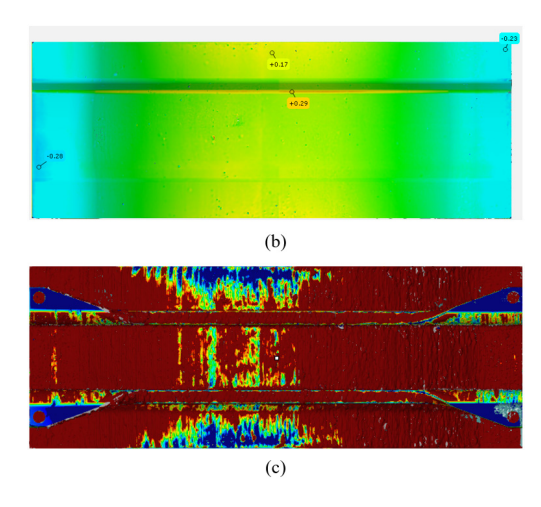


Figure 14. Comparison between nominal and actual geometry. The models were aligned by a local best fit on the top mold surface. All views share the same color scale shown on the isometric view. (a) Isometric view. (b) Top view of mold surface. (c) Bottom view with feet.

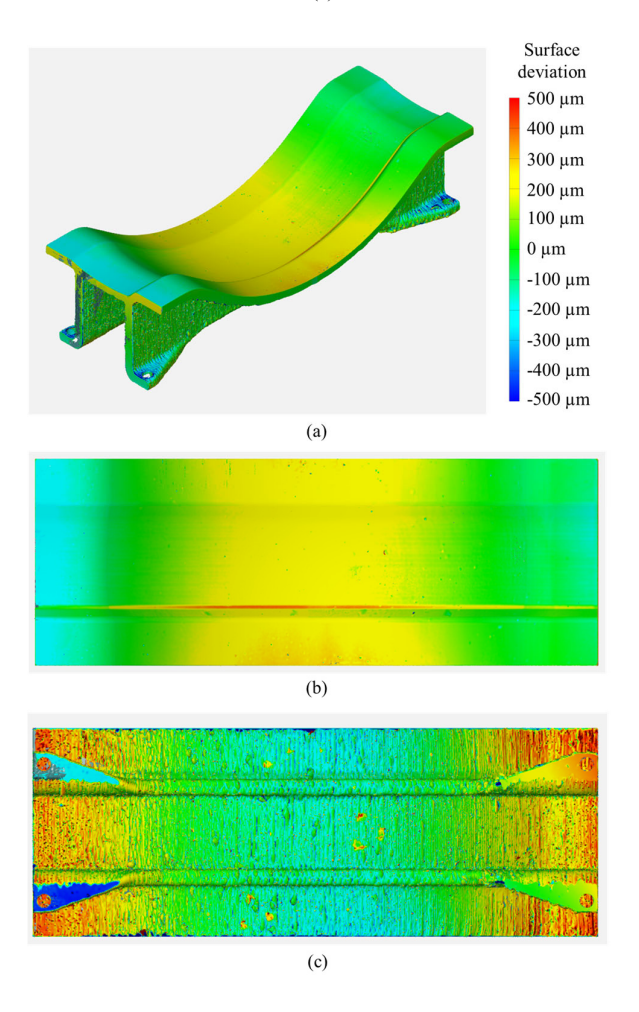


Figure 15. Comparison between the actual and predicted post-machining geometry. The models were aligned by a global best-fit on the entire part. All views share the same color scale shown on the isometric view. (a) Isometric view. (b) Top view of mold surface. (c) Bottom view with feet.

There are large deviations in the comparison to the nominal CAD, especially on the bottom. This is because of the extra

printed material left on non-machined surfaces. Other than this extra material, deviations are due to four primary factors discussed in the following subsections.

6.1. Mold surface fillet

There is one notable surface error caused by poor machining strategy. It will be discussed in brief to demonstrate that it is not associated with the scanning/fiducial methods described in this paper. The red horizontal stripe shown below in Figure 16 identifies extra material left on an internal fillet on the mold surface. There is approximately 150 µm of extra material left on this surface compared to the surrounding area. This occurred because the fillet radius (8 mm) was only slightly larger than the cutting tool radius (7.94 mm). When the tool entered this corner, the engagement with the part increased dramatically, which increased the cutting force and corresponding tool deflection.

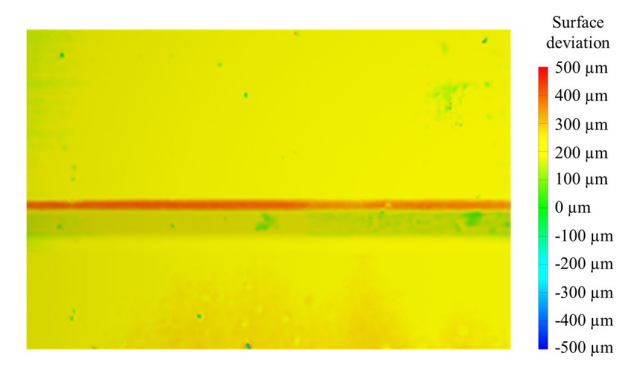


Figure 16. Surface deviation for a fillet on a mold surface. Note that while the color of the surface indicates a deviation of ${\sim}400~\mu m$ compared to the predicted stock model, the deviation relative to the surrounding material caused by tool deflection is only ${\sim}150~\mu m$.

This surface deviation can also be seen visually on the part. Figure 17 displays a closeup of the fillet; note the change in surface texture. This issue could be avoided by using a ball endmill with a smaller diameter to machine the fillet. This would reduce the engagement and cutting force.

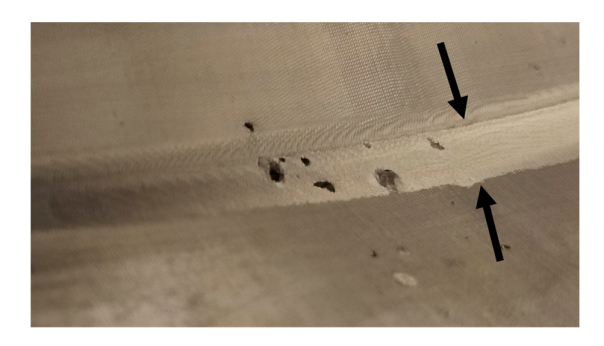


Figure 17. Closeup of surface deviation in a fillet on the mold face. The arrows point to the change in surface finish that occurred when the ball endmill entered the fillet and deflected.

6.2. Surface voids

There were many small holes (ranging from <1 mm to ~3 mm) present across the entire mold surface. The voids also appeared inside the waterjet cutouts in the part legs. Closeup views of voids are shown in Figure 18. Note how the voids in the waterjet cuts are present through the entire thickness of the part. Therefore, a deeper cut would not eliminate them.

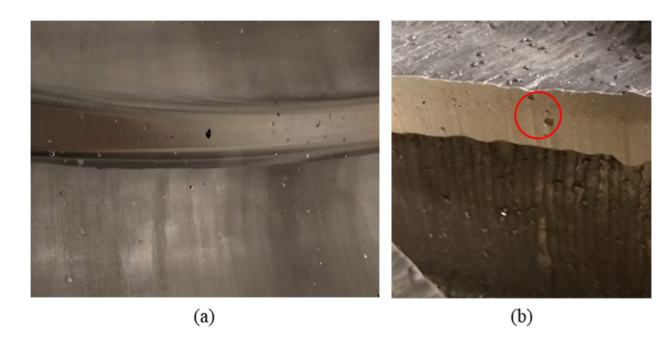


Figure 18. (a) Internal voids on mold surface. (b) Internal voids in waterjet cutouts on the legs.

Voids internal to the printed preform can be exposed during machining. Since the voids are inside the preform, they are not captured in the original scan and, therefore, are not modeled in the machining simulation. In-depth analysis of the causes of these internal voids is outside the scope of this paper. However, internal issues with the preform are clearly problematic since they affect the final part in ways that are difficult to predict.

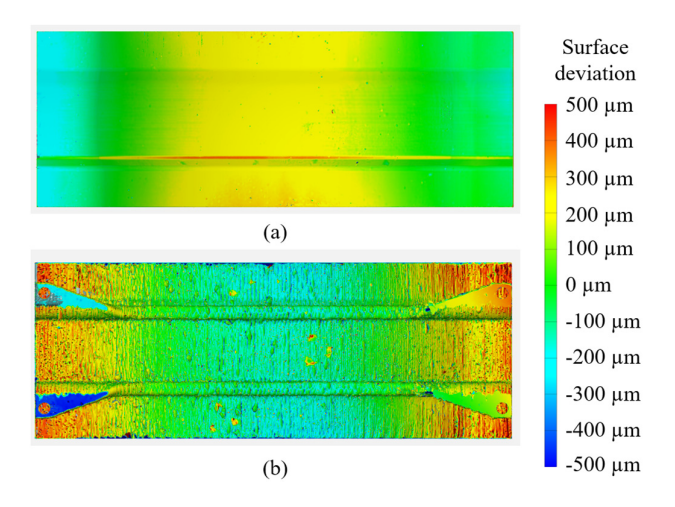


Figure 19. Distortion of the front (a) and back (b) sides of the mold due to internal stresses. Note how they show the same curvature, indicating that the entire mold is distorted rather than just the top surface.

6.3. Mold surface error

The mold surface shape showed a $500 \, \mu m$ deviation relative to the desired shape. This warp is attributed to internal stresses induced in the part during printing. When the part was machined, some of those internal stresses were released as material was removed, resulting in the part distortion. The key factor that points to this conclusion is that the back surface of the mold shows the same curvature relative to the initial scan.

If the part was bent due to workholding or the machining toolpaths were incorrect, this back surface wouldn't have changed shape. Figure 19 displays a comparison between the front and the back surfaces of the mold.

It is worth noting that this distortion occurred even though the part had been annealed before machining. The annealing was done using an annealing schedule specified by the end user for the part: the part was heated to 788 degrees C, held for 30 minutes for every 25 mm of part thickness (measured at the thickest part of the web, roughly 25 mm), and then air cooled. Despite this, there were still evidently internal stresses present in the material.

Note that the magnitude of the bend is somewhat different on the two sides ($400~\mu m$ on the front, $700~\mu m$ on the back). This is likely because, while some distortion occurred immediately as material was removed, some distortion was constrained by the workholding and only occurred after the part was unclamped. The immediate distortion on the top surface was re-machined during the finish pass and does not show up on the top surface. The top surface therefore shows only the delayed distortion that occurred after unclamping the part, while the bottom as-printed surface displays both the immediate and delayed distortion.

It would have been possible to re-machine the mold surface and remove this distortion. Since relatively little material would have to be removed during this re-finishing step, it would cause less warping than the original roughing and finish machining. This was not done since the part would be unusable due to the porosity.

6.4. Workholding distortion

There was notable deviation on the mold feet compared to the nominal, up to $500~\mu m$ as shown in Figure 20. The deviation is also not consistent across the different feet and it is not always in the same direction as the stress relieving error.

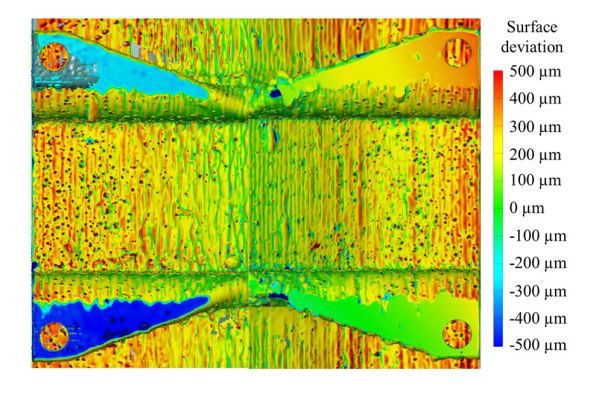


Figure 20: Surface deviation on the mold feet.

There was no particular tolerance on the feet so this is not a critical issue, but it is important to understand why this occurred. The source is elastic deformation of the part during the initial machining operation caused by the workholding. Since the clamps were not located directly at the locations where the part contacted the table, they deformed the part. The part was machined in this deformed state and, when released, the feet elastically recovered to a new position. This clamping

setup was necessary since the part was larger than the machine tool table. Figure 21 shows the workholding for this operation.

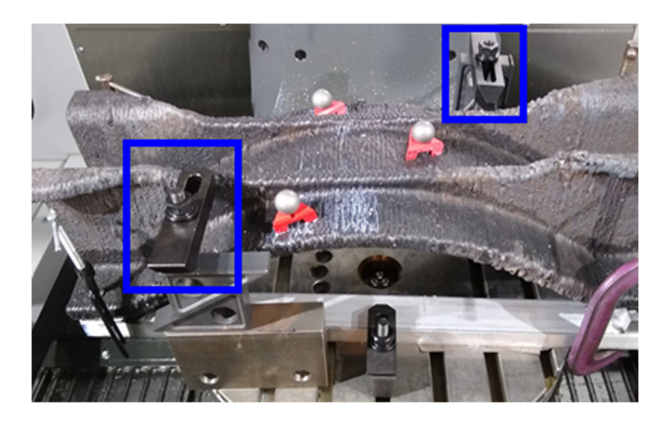


Figure 21: Workholding for the first machining operation. The two toe clamps (identified by blue squares) were not directly over the part supports, so the part elastically deformed in response to the clamping force.

7. Discussion

Generally, the fiducial-based coordinate system transfer strategy was successful. The optimal alignment of the CAD and preform was identified by scanning and this alignment was transferred from CAM to the machine. This method is simple to apply even for large and complex parts and has several clear advantages, including reduced process time. Full machining cycle time for this part was 12.5 hours, including roughing, finishing, and a final spring pass. The previous attempt to machine the part took nearly 51 hours of machining time before the part was scrapped and machining was aborted. This did not include finish machining. The vast majority of that time was spent in non-cutting motions that were necessary because the programmer had to assume a conservative amount of extra material on the entire part surface.

The final mold produced in this study was, ultimately, not usable due to internal voids revealed during the machining process. However, the results provide recommendations for future research on hybrid manufacturing processes. First, it is important to identify whether there are printing issues that could scrap the part prior to the machining process. Computed tomography (CT) could be implemented, for example, to reveal the internal geometry. This metrology will prevent wasted machining time on a part that cannot meet the design intentions.

Second, further study is required on how to mitigate internal stresses inside the part from the printing process. While residual stress and post-printing warping due to thermal gradients have been studied, there is little information on how to compensate for them during the machining process [20-21]. Further research on how to predict, prevent, and compensate for these stresses and the resulting warping is necessary.

Finally, part distortion due to workholding should be avoided. The scanning/fiducial method can be leveraged to detect and avoid part distortion, either by rescanning the part while clamped and comparing the geometry to the free-state scan, adding redundant fiducials to the part and comparing the scanned free-state positions to the probed clamped positions, or by local compensation of the machining toolpaths [18].

8. Conclusions

This paper demonstrated a method for transferring five-axis machining coordinate systems using structured light scanning to identify the positions of fiducials relative to an additively manufactured preform. This method can improve accuracy, reduce scrap, and lower machining cycle time. For the Invar wire arc additive preform studied here, however, the final machined part was unusable due to a combination of warping due to internal stresses and porosity from the printing process. Several key recommendations were made based on these results for future work. In continuation of this effort, a new preform will be printed to reduce internal porosity and the fiducial-based machining strategy will be repeated.

9. Acknowledgements

The work reported here was in collaboration with GKN Aerospace and was partially supported through the Manufacturing and Materials Joining Innovation Center (Ma²JIC) University of Tennessee, Knoxville site. Ma²JIC is funded by the National Science Foundation (NSF) through the Industry/University Cooperative Research Center (I/UCRC) program award number IIP 1822186.

This manuscript has been funded by UT-Battelle, LLC, under contract DE-AC05-00OR22725 with the US Department of Energy (DOE). The US government retains and the publisher, by accepting the article for publication, acknowledges that the US government retains a nonexclusive, paid-up, irrevocable, worldwide license to publish or reproduce the published form of this manuscript, or allow others to do so, for US government purposes. DOE will provide public access to these results of federally sponsored research in accordance with the DOE Public Plan Access (http://energy.gov/downloads/doe-public-access-plan).

Appendix A. MATLAB code for coordinate system transformation

This appendix provides the MATLAB script used to transfer the work coordinate system from the machine to CAM.

```
clear
% Probed sphere positions in machine
coordinates.
% They identify the top apex, not the center
point.
sphere1 =
          [-401.589 -158.267 -326.896];
sphere2 = [-306.846 - 298.259 - 309.750];
sphere3 = [-209.784 - 183.371 - 330.626];
% Compensate for the radius of the spheres in
Z direction.
sphere1 = sphere1 - [0 0 12.7];
sphere2 = sphere2 - [0 \ 0 \ 12.7];
sphere3 = sphere3 - [0 0 12.7];
% Calculate fiducial coordinate system
P fid = sphere1;
datXVec = (sphere2-sphere1) / (norm(sphere2-
sphere1));
sphere3Vec = sphere3-sphere1;
```

```
dat3XCoord = dot(sphere3Vec, datXVec);
datYVec = (sphere3Vec - (dat3XCoord *
datXVec)) / norm(sphere3Vec - (dat3XCoord *
datXVec));
datZVec = cross(datXVec, datYVec);
O fid = [datXVec' datYVec' datZVec'];
% Find the machine fiducial system
O_mach = transpose(O_fid);
% Calculate the vectors to reconstruct in CAM
machXInFid = 50 * O_mach(:,1)
machYInFid = 50 * 0 mach(:,2)
machZInFid = 50 * 0 mach(:,3)
% Calculate the clamping position for CAM
MRZPCenter = [-325.785 -254.574 -475.308]; %
Calibrated Machine Rotation Zero Point
tableCenterToMRZP = [0 0 50.8]; % Offset
between MRZP and the CAM clamp point
clampingPosition = transpose(MRZPCenter -
sphere1 - tableCenterToMRZP)
```

References

- [1] Sahoo, K.C. and Menq, C.H., 1991. Localization of 3-D objects having complex sculptured surfaces using tactile sensing and surface description.
- [2] Cornelius, A., Dvorak, J., Jacobs, L., Penney, J. and Schmitz, T., 2021. Combination of structured light scanning and external fiducials for coordinate system transfer in hybrid manufacturing. Journal of Manufacturing Processes, 68, pp.1824-1836.
- [3] Lamsey, M., 2021. Design and Fabrication of Invar Layup Tool Molds using Additive and Subtractive Manufacturing. Thesis, University of Tennessee, Knoxville.
- [4] Dávila, J.L., Neto, P.I., Noritomi, P.Y., Coelho, R.T. and da Silva, J.V.L., 2020. Hybrid manufacturing: A review of the synergy between directed energy deposition and subtractive processes. The International Journal of Advanced Manufacturing Technology, pp.1-14.
- [5] Zhu, Z., Dhokia, V.G., Nassehi, A. and Newman, S.T., 2013. A review of hybrid manufacturing processes – State of the art and future perspectives. International Journal of Computer Integrated Manufacturing, 26(7), pp.596-615.
- [6] Stavropoulos, P., Souflas, T. and Bikas, H., 2021. Hybrid manufacturing processes: An experimental machinability investigation of DED produced parts. Procedia CIRP, 101, pp.218-221.
- [7] Chen, N., Barnawal, P. and Frank, M.C., 2018. Automated post machining process planning for a new hybrid manufacturing method of additive manufacturing and rapid machining. Rapid Prototyping Journal.
- [8] Liou, F., Slattery, K., Kinsella, M., Newkirk, J., Chou, H.N. and Landers, R., 2007. Applications of a hybrid manufacturing process for fabrication of metallic structures. Rapid Prototyping Journal, 13(4), pp.236-244.
- [9] Yamazaki, T., 2016. Development of a hybrid multi-tasking machine tool: Integration of additive manufacturing technology with CNC machining. Procedia CIRP, 42, pp.81-86.
- [10] Song, Y., Park, S., Choi, D., and Jee, H., 2005. 3D welding and milling: Part I – A direct approach for freeform fabrication of metallic prototypes. International Journal of Machine Tool and Manufacture, 45(9), pp.1057-1062
- [11] Eiríksson, E.R., Wilm, J., Pedersen, D.B. and Aanæs, H., 2016. Precision and accuracy parameters in structured light 3-D scanning. International Archives of the Photogrammetry, Remote Sensing and Spatial Information Sciences, 5, p.W8.
- [12] Gebler, O.F., Goudswaard, M., Hicks, B., Jones, D., Nassehi, A., Snider, C. and Yon, J., 2021. A COMPARISON OF STRUCTURED LIGHT SCANNING AND PHOTOGRAMMETRY FOR THE DIGITISATION OF PHYSICAL PROTOTYPES. Proceedings of the Design Society, 1, pp. 11-20.
- [13] Ghandali, P., Khameneifar, F. and Mayer, J.R.R., 2019. A pseudo-3D ball lattice artifact and method for evaluating the metrological performance of

- structured-light 3D scanners. Optics and Lasers in Engineering, 121, pp.87-95.
- [14] Naidu, J., Phan, V.A. and Nguyen, N.Q., 2021. Endoscopic Ultrasound-Guided Fiducial Marker Placement for Stereotactic Body Radiotherapy (SBRT) of Pancreatic Cancer. In Endoscopic Ultrasound Management of Pancreatic Lesions (pp. 165-178). Springer, Cham.
- [15] Khullar, K., Dhawan, S.T., Nosher, J. and Jabbour, S.K., 2021. Fiducial marker migration following computed tomography-guided placement in the liver: a case report. AME Case Reports, 5.
- [16] Smith, S., Woody, B.A. and Miller, J.A., 2005. Improving the accuracy of large scale monolithic parts using fiducials. CIRP annals, 54(1), pp.483-486.
- [17] Wang, S., Cheung, C., Ren, M. and Liu, M., 2018. Fiducial-aided on-machine positioning method for precision manufacturing of optical freeform surfaces. Optics express, 26(15), pp.18928-18943.
- [18] Liu, H.B., Hou, B., Zhang, J. and Wang, Y.Q., 2015, August. Improving Machining Accuracy of Thin-Wall Parts Using the Information-Localizing Technology. In International Conference on Intelligent Robotics and Applications (pp. 701-709). Springer, Cham.
- [19] Srinivasan, H., Harrysson, O.L. and Wysk, R.A., 2015. Automatic part localization in a CNC machine coordinate system by means of 3D scans. The International Journal of Advanced Manufacturing Technology, 81(5), pp.1127-1138.
- [20] Shen, C., Reid, M., Liss, K.D., Pan, Z., Ma, Y., Cuiuri, D., van Duin, S. and Li, H., 2019. Neutron diffraction residual stress determinations in Fe3Al based iron aluminide components fabricated using wire-arc additive manufacturing (WAAM). Additive Manufacturing, 29, p.100774.
- [21] Szost, B.A., Terzi, S., Martina, F., Boisselier, D., Prytuliak, A., Pirling, T., Hofmann, M. and Jarvis, D.J., 2016. A comparative study of additive manufacturing techniques: Residual stress and microstructural analysis of CLAD and WAAM printed Ti–6Al–4V components. Materials & Design, 89, pp.559-567.